# Local Microstructural Modification in Dynamically Consolidated Metal Powders

W. H. GOURDIN

Powders of 4330V steel, aluminum-6 pct silicon, and copper have been dynamically consolidated under well-characterized conditions using shock waves. Different regions in the final microstructures correlate well with the shock conditions during compaction, demonstrating the importance of the shock history in determining the final microstructure. Martensite is observed to form locally at powder particle surfaces in compacts of 4330V steel, and interparticle melting and rapid resolidification are observed in compacts of aluminum-6 pct silicon. Microprobe analyses of locally melted regions in the aluminum alloy indicate a homogeneous distribution of 6 pct silicon, well above the maximum equilibrium solid solubility. Comparison with the structure of "splat caps," found in the starting powder, suggests that locally melted regions experience a cooling rate comparable to that obtained in splat quenching. The extent of martensite formation and local melting are in good agreement with current models for energy deposition at powder particle surfaces during consolidation. The general implications of the analysis and observations are discussed.

## I. INTRODUCTION

DYNAMIC consolidation is currently of considerable interest as a means of forming monolithic bodies from rapidly solidified or metastable powders.[1-10] The technique, in which shock waves are used to mechanically drive the powder to high density, is unique in that energy is deposited primarily at particle interfaces.[11] This can restrict accompanying microstructural changes in powder particles to the near-surface region, producing localized melting and phase transformation[1-7] without substantial alteration of the interior.

In this paper, the microstructures of dynamically compacted 4330V steel, aluminum-6 pct silicon, and copper powders, formed under well-characterized conditions, are presented and discussed in terms of an energy flux model of energy deposition during consolidation.[11,12] The experiments explore a range of relevant compaction conditions and material and powder properties. The material characteristics and experimental details are first briefly considered, followed by a presentation of the microstructural observations. These observations are analyzed in terms of both the known shock history of the specimens and the energy deposited in the powder. The implications of the observations and analysis are then discussed, with particular regard to the influence of powder characteristics on the final microstructure.

## II. EXPERIMENTAL

### A. *Starting Materials*

Three powders were studied: inert gas atomized 4330 vanadium-modified steel (4330V), ultrasonically atomized aluminum-6 pct silicon alloy, and irregular copper. These were chosen to represent a range of material and powder characteristics, summarized in Tables I and II, respectively. Dynamic consolidation of a spherical copper powder is considered elsewhere.[11,13]

1. *4330V*

The optical microstructure of the as-received 4330V powder is shown in Figure 1 and consists of fine laths of martensite similar to those observed in oil-quenched 4340 steels.[14] X-ray diffraction analysis shows a small amount of retained austenite as well. Scanning electron micrographs reveal a generally spherical particle shape, with small (5 to 20 $\mu$m) spherical nodules on the surface of many powder particles (Figure 1). These nodules apparently separate individual particles, an effect which, together with a limited size distribution, reduces the packing density to only 50 pct of the solid density (Table II).

2. *Aluminum-6 pct silicon*

The structure of the aluminum-6 pct silicon alloy powder is shown in Figure 2. Surface nodules are present, as in the steel, but the large fraction of fine particles yields a higher packing density (Table II). The optical microstructure consists of a distinctive pattern of silicon precipitates surrounding aluminum cells. X-ray diffraction analysis indicates that the amount of silicon in solid solution in these cells does not exceed the maximum equilibrium solid solubility, about 1.65 wt pct.[15] As shown in Figure 2, however, some of the larger particles have at their surfaces the remnants of liquid droplets struck by already-solidified powder particles during the atomization process. Microprobe analysis (Figure 3) shows that these "splat caps" contain approximately the same average amount of silicon as the surrounding particles, but that fluctuations in the silicon content are substantially less, indicating a much more homogeneous distribution. Some structure is apparent within the splat cap, however (Figure 3(a)), and it is not clear whether the microstructure consists of a metastable solid solution or merely a distribution of fine silicon precipitates. Nevertheless, these observations suggest that such regions experienced significantly more rapid cooling than the particles themselves.

3. *Copper*

The copper powder is distinguished by its very low packing density and irregular sponge-like character, shown in the

W. H. GOURDIN is a Physicist with Lawrence Livermore National Laboratory, Livermore, CA 94550.

Manuscript submitted October 31, 1983.

**Table I. Material Properties**

| Properties | 4330V | Al + 6 Pct Si | Copper |
|---|---|---|---|
| Composition (wt pct) | 0.3 C, 1.8 Ni, 0.8 Cr, 0.4 Mo, 0.07 V, bal Fe | 7.3 Si bal Al | Cu |
| Density ($10^3$ kg/m$^3$) | 7.84 | 2.69 | 8.92 |
| Melting temperature (°C) | 1452 to 1563 | 577[a] to 615 | 1084 |
| Specific heat ($10^3$ J/kg − °K) | 0.67 | 1.05 | 0.438 |
| Thermal conductivity: solid | 0.5 | 2.3 | 3.7 |
| ($10^2$ W/m − °K) liquid | 0.5 | 1.0 | 1.1 |
| Thermal diffusivity: solid | 0.096 | 0.82 | 0.95 |
| ($10^{-4}$ m$^2$/s) liquid | 0.096 | 0.35 | 0.28 |
| Latent heat ($10^5$ J/kg) | 2.7 | 4.0 | 2.05 |
| Martensite temperature, $M_s$(°C) | 302 | — | — |

[a]Eutectic temperature

**Table II. Powder Characteristics**

| Characteristics | 4330V | Al + 6 Pct Si | Copper |
|---|---|---|---|
| Packing density: ($10^3$ kg/m$^3$) | 3.89 | 1.81 | 2.73 |
| (pct solid) | 50 | 67 | 31 |
| Morphology | spherical | spherical | irregular |
| Particle size range ($\mu$m) | −177 + 44 | −250 | −125 + 63 |
| Median particle size ($\mu$m)[a] | 70 | 30 | 70 |
| Specific surface (m$^2$/kg)[b] | 32 | 145 | 94 |
| Area-equivalent diameter, $\mathcal{D}$ ($\mu$m) | 23.9 | 15.4 | 7.15 |

[a]Sieve size
[b]BET method

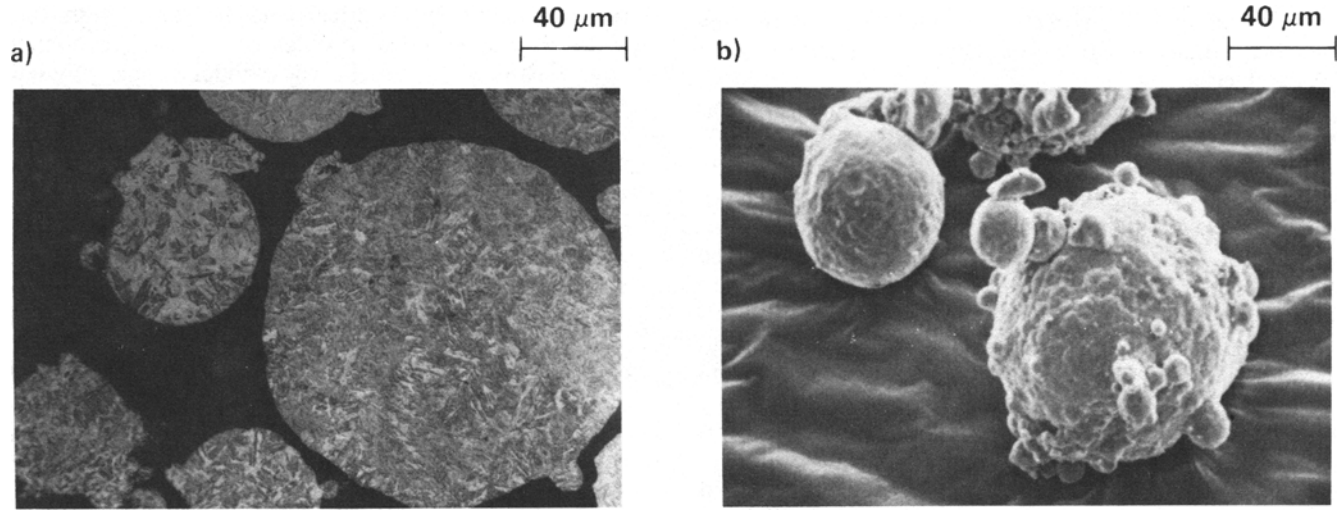


Fig. 1 — Microstructure of the 4330V steel powder: (*a*) optical micrograph, nital etch; (*b*) scanning electron micrograph.

micrographs of Figure 4. Small particles are agglomerated to form a highly porous mass that has a large specific area.

### B. *Compaction Experiments*

The compaction assembly used in these experiments, shown in Figure 5, was designed to produce an initially planar, one-dimensional shock in the first 2 mm of the powder specimen. The powder was placed in a cavity 8 mm deep by 57 mm in diameter machined in a 50-mm-thick block of mild or 304 stainless steel. A planar shock generated by an explosive was transmitted to the powder through a 6.35-mm-thick copper driver plate. The stress history of the specimen was modified in some experiments by a 1.5-mm-thick mild steel plate placed between the copper driver and the powder. This steel plate undergoes a phase transformation at 13.0 GPa[16] which produces multiple shock states in the powder, discussed in more detail subsequently. This effect is eliminated by using a 0.13-mm-thick 304 stainless steel cover, which does not undergo a phase transformation and has an excellent acoustical impedance match with the copper driver. The thin cover is necessary to prevent extrusion of the copper into the interstices at the surface of the powder specimen.

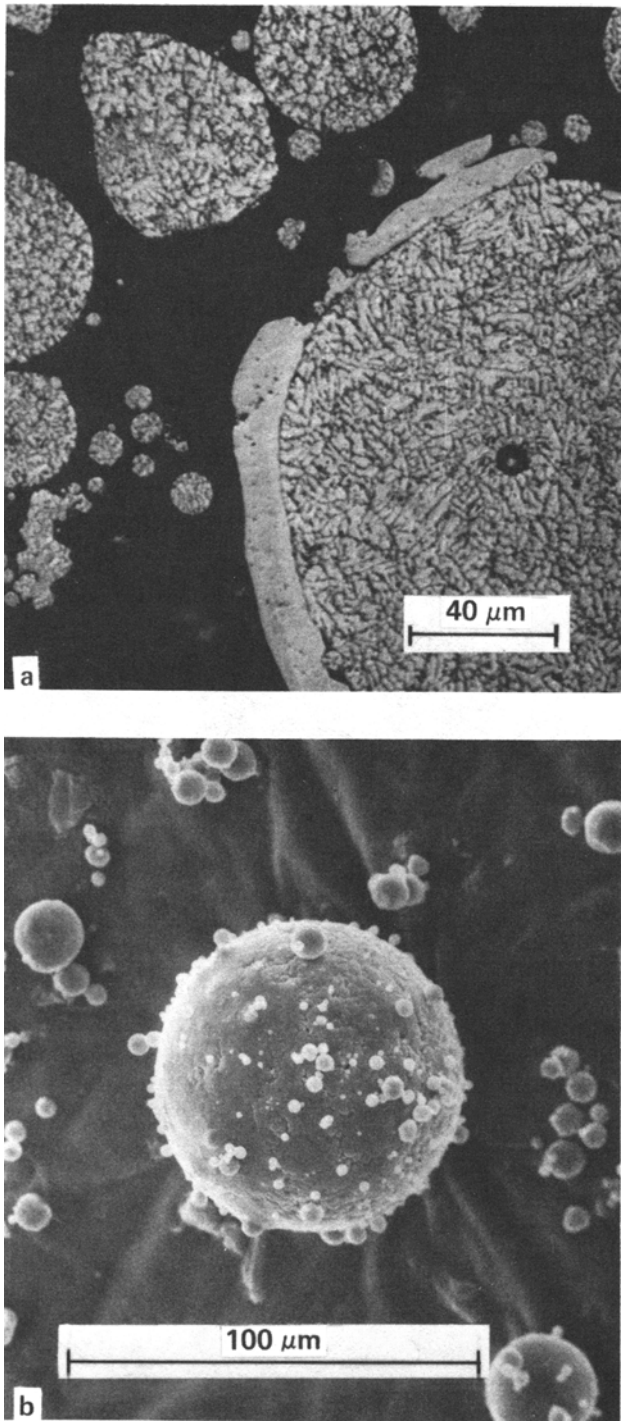


Fig. 2—Microstructure of the aluminum-6 pct silicon alloy powder: (*a*) optical micrograph, sodium hydroxide etch; (*b*) scanning electron micrograph showing surface nodules similar to those found on the steel powder particles. Optical micrograph courtesy J. E. Smugeresky.

Two well-characterized explosives[17] at three densities were used in these experiments (Table III). Equations of state are available for these materials,[17,18] making possible reliable calculations of the stresses produced in the copper driver and powder specimen. To verify these calculations, calibration experiments were performed to measure the stress delivered to the copper driver plate. These results are

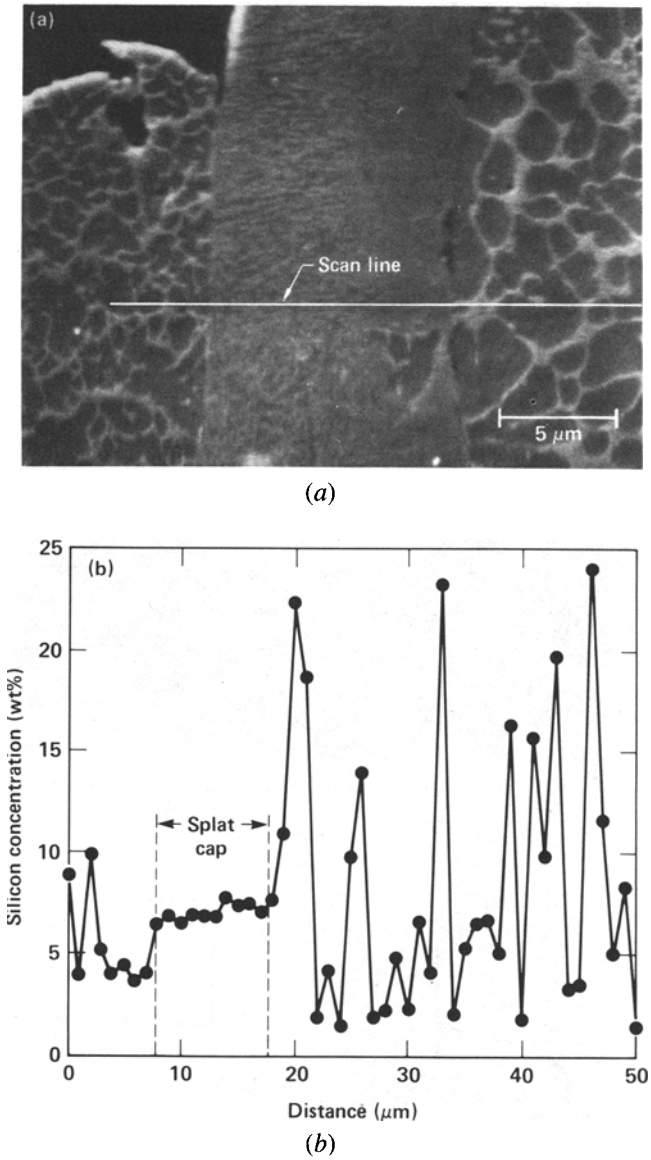


Fig. 3—Microprobe scan of a "splat cap." (*a*) Scanning electron micrograph showing the scan line. The splat region shown lies on the surface of a 65 μm diameter particle at right. The 10 μm particle at left provides a convenient endpoint for the microprobe scan. (*b*) Silicon distribution along the scan line. The silicon distribution in the splat cap is more homogeneous than in the particles themselves.

also summarized in Table III, and the agreement with calculation is excellent. Variations in the compaction stresses produced by a single type of explosive can occur because of slight differences in packing. Such small deviations can be estimated from the changes observed in the measured detonation velocities.[19]

### C. *Metallographic Specimen Preparation*

Standard techniques were used in the preparation of metallographic specimens. Because of the curvature* of the compacts it was generally possible to section them only in a plane perpendicular to the shock front. This allowed easy

*Bending of the specimen occurs only after the initial shock has passed through, and compacted, the powder.

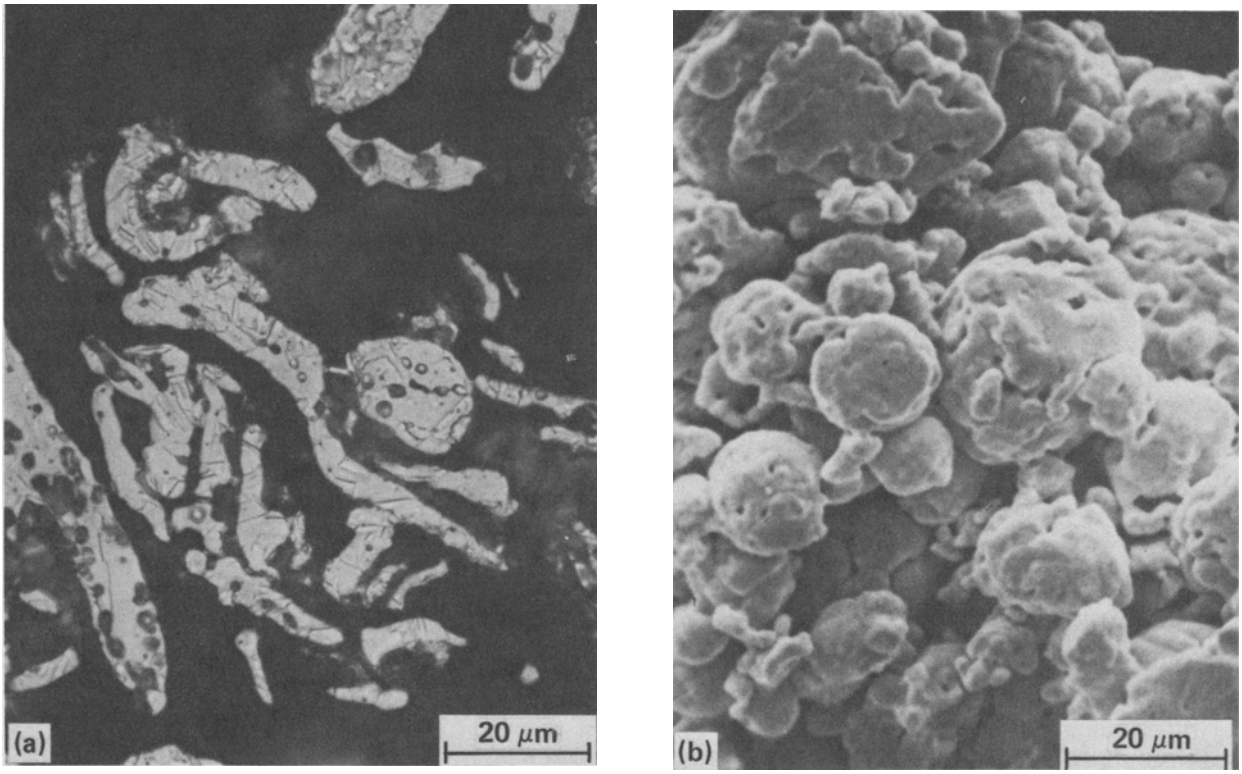


Fig. 4 — Microstructure of the copper powder: (*a*) optical micrograph; (*b*) scanning electron micrograph. Small powder particles form aggregates that have a very large specific area.

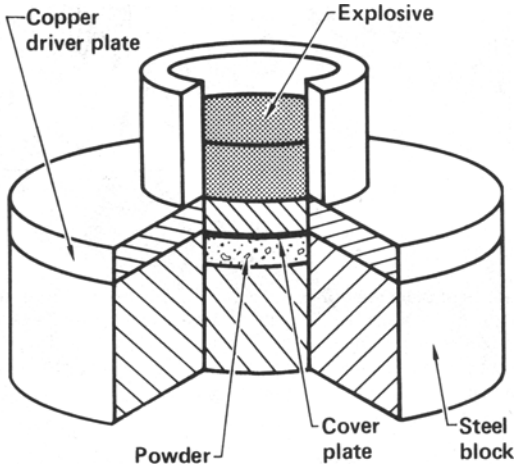


Fig. 5 — Assembly used in the explosive experiments. Approximately 200 g of explosive were packed into an acrylic container 57 mm in diameter. The explosive was detonated with a 56-mm plane wave lens and the detonation velocity was measured with two sets of shorting pins on either side of the container.

observation, near the axis of the specimens, of the effects of a simple one-dimensional shock. However, one specimen (3P, Table IV) was sectioned parallel to the shock front as well, at a depth corresponding approximately to the region of maximum shock stress. The measured amount of transformed material in this plane was determined by a lineal analysis to be about 21 pct. Given the uncertainties of measurement, this corresponds reasonably well with values obtained from sections perpendicular to the shock front (26 to 32 pct, Table IV). It is concluded that asymmetries in the distribution of the shock-induced structure are not large.

**Table III. Explosive Characteristics**

| Type | Density ($10^3$ km/m$^3$) | $v_d$[a] (km/s) | Stress in Copper Driver: Calculated[b] (GPa) | Stress in Copper Driver: Measured[c] (GPa) |
|---|---|---|---|---|
| PETNA | 0.88 | 4.86 | 15.0 | 12.9 |
| PETNB | 0.95 | 5.34 | 16.0 | 14.8 |
| HMX | 1.15 | 6.31 | 20.0 | 19.0 |

[a]Detonation velocity
[b]Calculated at the explosive copper interface
[c]Measured after traversing 6.35 mm of copper

## III. RESULTS

All specimens were cracked to some degree, the result of radial and axial stress release as well as late-time distortion of the compaction fixture. Such cracking had no significant effect on the microstructural observations of interest here, and no attempt was made to optimize the compaction assembly to eliminate it. Cracking does reduce the density of the compacts, so that the measured average densities given in Tables IV, V, and VI may be slightly less than those of the solids even at the highest stresses. However, the stress at which complete densification is achieved can be inferred from Hugoniot data.[19,20]*

*The Hugoniot is the locus of stress-volume states achieved upon shock loading. See References 11 and 20 and the references therein.

**Table IV. 4330V Experimental Conditions and Comparison with Calculations**

| Exp. | Expl. | Average Final Density ($10^3$ kg/m$^3$) | Region | Stress (GPa) | $E$ ($10^5$ J/kg) | Flux ($10^{11}$ W/m)$^2$ | Residual Temp. $E/Cp$ (°C) | Calculated Maximum Surface Temp. $T_s$ (°C) | Calculated Extent of Melting (Vol Pct) | Extent of Transformation (Vol Pct) Measured[a] | Calculated[b] |
|---|---|---|---|---|---|---|---|---|---|---|---|
| 1P | PETNA | 7.38 | — | 2.4 | 1.60 | 0.79 | 239 | 1486 | 0 | NM | 13 |
| 2P[d] | PETNB | 7.65 | I | 2.85 | 1.60 | 0.88 | 239 | 1562[c] | 2 | NM | 14 |
| | | | II | 3.85 | 2.21 | 1.41 | 330 | 2125 | 7 | 21 (11) | 21 |
| | | | III | 3.6 | 2.06 | 1.25 | 308 | 1942 | 5.5 | | 19 |
| 3P[d] | HMX | 7.66 | I | 2.7 | 1.64 | 0.88 | 245 | 1588[c] | 2 | NM | 14 |
| | | | II | 5.55 | 3.55 | 2.68 | 531 | 3736 | 15.5 | 32 (26 to 28) | 36 |
| | | | III | 4.8 | 3.06 | 2.125 | 451 | 3097 | 13 | | 30 |
| 17P | PETNB | 7.70 | — | 2.9 | 1.92 | 1.05 | 287 | 1730 | 4 | NM | 17 |
| 18P | HMX | 7.53 | — | 4.7 | 3.12 | 2.17 | 466 | 3129 | 13 | NC | 31 |

[a]The first values are from lineal analyses. Values in parentheses were obtained by Quantimet® image analysis. NM means transformed material was observed but the volume fraction was too small to measure. NC means contrast was not sufficient for a satisfactory analysis.
[b]807 °C isotherm
[c]Latent heat neglected
[d]Mild steel cover plate

**Table V. Aluminum-6 Pct Silicon Experimental Conditions and Comparison with Calculations**

| Exp. | Expl. | Average Final Density ($10^3$ kg/m$^3$) | Region | Stress (GPa) | $E$ ($10^5$ J/kg) | Flux ($10^{11}$ W/m)$^2$ | Residual Temp. $E/Cp$ (°C) | Calculated Maximum Surface Temp. $T_s$ (°C) | Extent of Melting (Vol Pct) Measured | Calculated[a] |
|---|---|---|---|---|---|---|---|---|---|---|
| 7P[c] | PETNA | 2.61 | — | 1.75 | 1.53 | 0.61 | 146 | 435 | <1 | 0 |
| 11P[c] | PETNB | 2.65 | I | 1.88 | 1.71 | 0.69 | 163 | 485 | 0 | 0 |
| | | | II | 2.55 | 2.36 | 1.10 | 225 | 700 | 6 | 4 |
| 15P[c] | HMX | 2.65 | II | 4.00 | 3.60 | 2.09 | 343 | 1158 | 16 | 17 |
| 16P | PETNB | 2.63 | — | 2.35 | 2.22 | 0.985 | 211 | 647 | <1 | 2 |
| 19P | HMX | 2.64 | — | 3.45 | 3.18 | 1.71 | 302 | 993 | NC[b] | 13 |

[a]577 °C isotherm
[b]Contrast not great enough to permit measurement.
[c]Mild steel cover plate. In 7P the stress in the cover was less than the transformation stress of 13.0 GPa. State I in 15P is the same as state I in 11P.

**Table VI. Irregular Copper Experimental Conditions and Comparison with Calculations**

| Exp. | Expl. | Average Final Density ($10^3$ kg/m$^3$) | Region | Stress (GPa) | $E$ ($10^5$ J/kg) | Flux ($10^{11}$ W/m)$^2$ | Residual Temp. $E/Cp$ (°C) | Calculated Maximum Surface Temp. $T_s$ (°C) | Extent of Melting (Vol Pct) Measured | Calculated[a] |
|---|---|---|---|---|---|---|---|---|---|---|
| 10P[a] | PETNB | 8.84 | I | 1.48 | 1.85 | 0.25 | 422 | 495 | 0 | 0 |
| | | | II | 2.08 | 2.57 | 0.41 | 587 | 691 | 0 | 0 |

[a]Mild steel cover plate

A. *4330V*

The results of experiments on the 4330V steel powder are summarized in Table IV. Although all the final densities are near the solid value, complete densification is not achieved for compaction stresses less than about 3.0 GPa.[11,19,20] As the stress is increased, the compacts become increasingly well bonded, and all specimens except 1P show good integrity despite cracking.

Compacts formed at stresses below 3.0 GPa show little evidence of either interparticle bonding or microstructural modification. Close examination of the microstructure of specimen 1P reveals thin, 1 to 5 $\mu$m, layers of what appears to be martensite between some powder particles (Figure 6), but such layers are not a dominant feature of the microstructure.[19]

The microstructures of samples 2P and 3P, Figures 7 and 8, are clearly divided into three regions near the impact face. The initial region, immediately adjacent to the impact face in contact with the mild steel cover plate, shows no obvious thermal modification. Its thickness decreases with increasing shock stress, from 150 to 200 $\mu$m for 2P (Figure 7) to about 70 to 100 $\mu$m (one median particle diameter) for 3P (Figure 8).

The second region contains substantial amounts of untempered martensite, formed locally at the interfaces between unaltered powder particles, a microstructure similar to that observed by Morris.[7,21] Microhardness measurements show the martensite to have a hardness of 644 kg/mm$^2$, comparable to the hardness of untempered martensite in quenched wrought steels,[22] but significantly greater than the hardness of the particle interiors (456 kg/mm$^2$). The amount of martensite increases with increasing stress and forms a continuous interparticle phase in 3P (Figure 8). Lineal analysis shows that 21 pct by volume of the powder has been transformed in 2P and 32 pct in 3P. Image analysis gives somewhat smaller values (Table IV). Although it is assumed here that all of the austenite which forms locally is converted to martensite, some "tempering" may result from slower local cooling rates or higher residual temperatures.

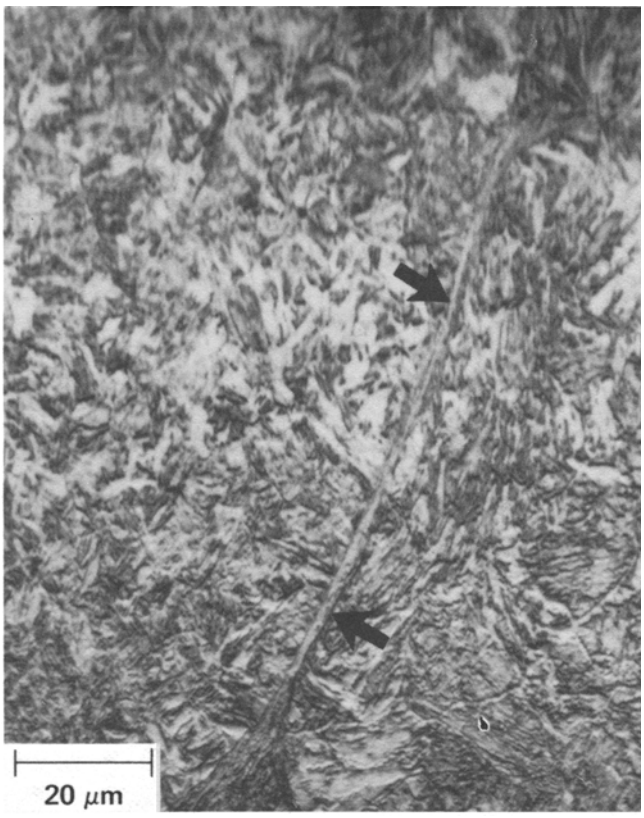


Fig. 6 — Microstructure of specimen 1P, showing what appears to be a thin zone of modified material (arrows) at a powder particle interface. The structure of the particle interior is unchanged.

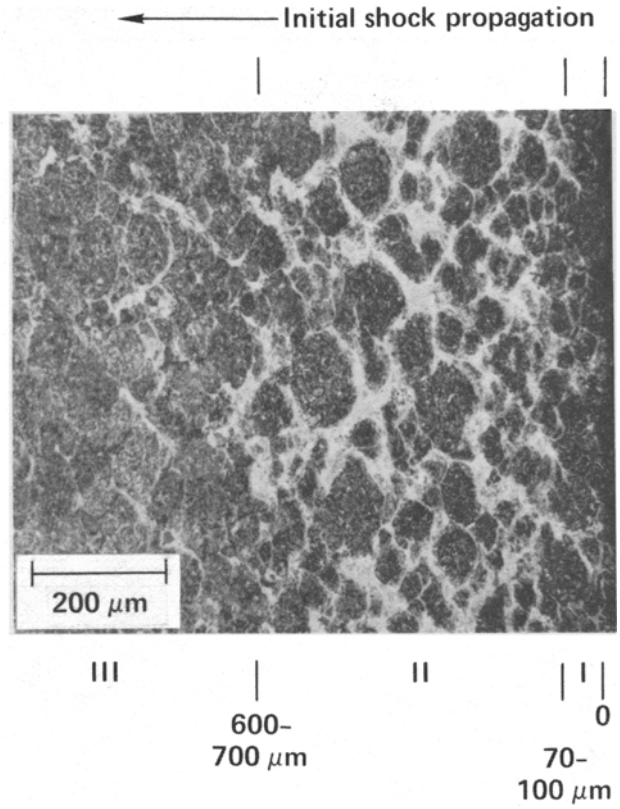


Fig. 7 — Microstructure of specimen 2P. The formation of three regions near the impact face is caused by the phase transformation in the mild steel cover plate used in this experiment. The stress in the copper driver was 15.0 GPa. White areas are untempered martensite. Etched with nital.

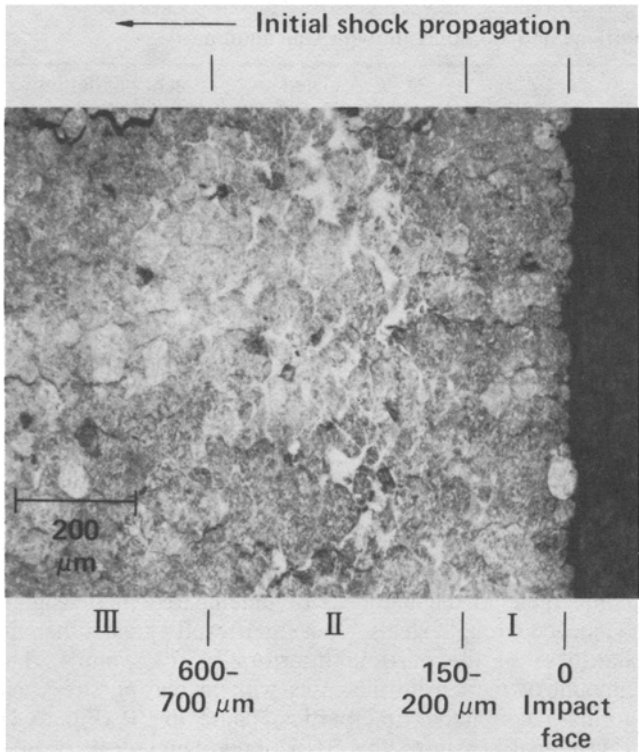


Fig. 8 — Microstructure of specimen 3P, for which the stress in the copper driver was 19.0 GPa. The higher stress relative to 2P produces a thinner region I and significantly more martensite formation in region II.

Close examination of martensitic regions in 3P (Figure 9) reveals structure which may indicate such an effect.

The third region in these specimens begins 600 to 700 μm from the impact face and consists of a gradually diminishing amount of interparticle martensite dispersed between otherwise unaltered particles. It is significant that this depth, unlike the thickness of the first region, does not appear to be a strong function of the stress level.

Experiments without the steel cover plate (17P, 18P) do not show the initial region at the impact face. Sample 18P shows considerable modification (Figure 10), but the interparticulate material has the appearance of a tempered martensite, possibly the result of a high residual temperature.[19] The thickness of the altered region is 600 to 800 μm, comparable to the combined thickness of the first two regions in samples 2P and 3P.

Direct evidence for interparticle melting within particles was not found in any of the steel compacts. However, the good integrity of several specimens formed at higher stresses indicates that some localized melting may have occurred. The extent of melting estimated using the energy flux model,[11] described subsequently, is summarized in Table IV.

### B. *Aluminum-6 Pct Silicon*

Experiments with the aluminum-6 pct silicon powder[6,11,19] show that at stresses below 1.7 GPa no substantial bonding or microstructural modification occurs. For stresses above 1.7 GPa (Table V), however, regions of locally modified

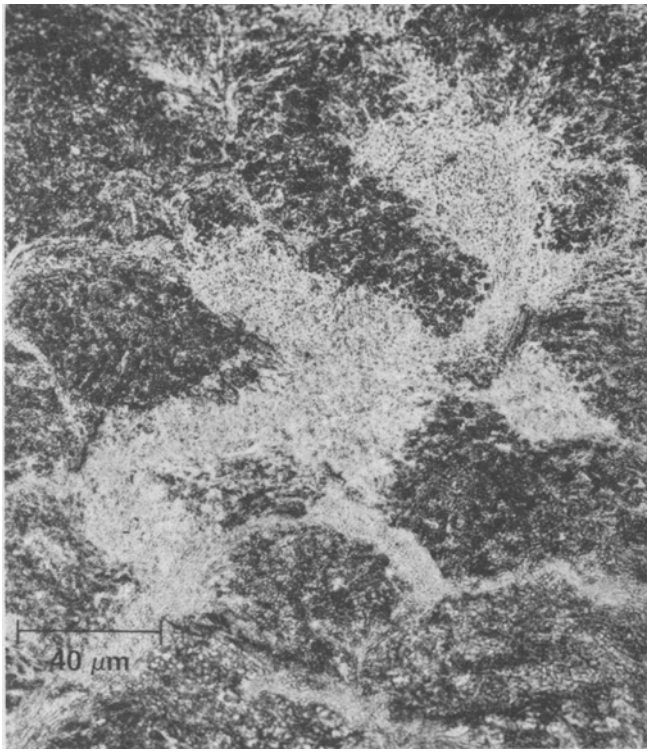


Fig. 9—Detail of martensitic region in specimen 3P.

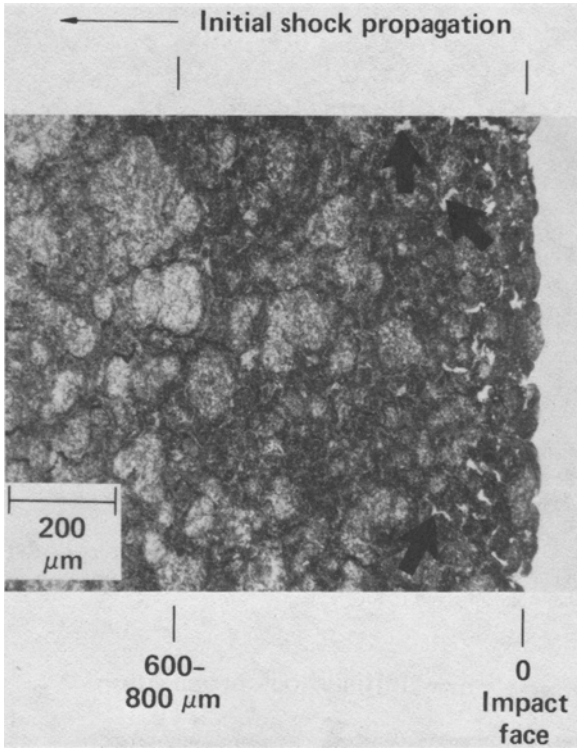


Fig. 10—Microstructure of specimen 18P, compacted under nominally the same conditions as 3P, but with a thin 304 stainless steel cover rather than mild steel. This eliminates the triplex structure seen in Figs. 7 and 8, but the stainless steel has extruded into pores near the surface. Although significant microstructural change has occurred, only a few regions appear to be martensite (arrows).

material begin to appear at powder particle interfaces. These regions, an example of which is shown in Figure 11, have an internal structure similar to that of the splat caps observed in the starting powder, but are distinguished by their irregular appearance and intimate association with surrounding particles of unaltered microstructure. A microprobe scan of a modified region in sample 11P, shown in Figure 12, reveals a much more homogeneous distribution of silicon than in the surrounding particles and quantitative analysis[19]

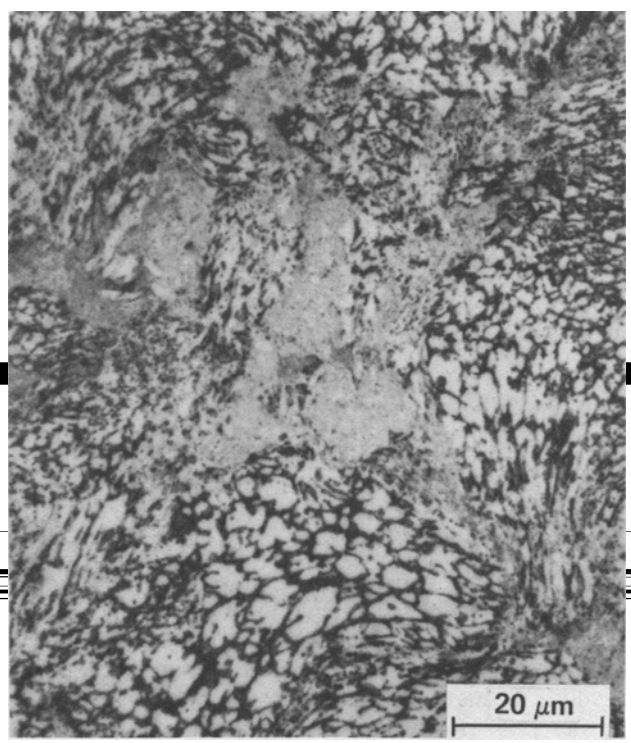


shows an average silicon content within the modified zone of 6.0 to 6.5 pct. These observations indicate that the modified material has melted and resolidified rapidly during consolidation. Comparison with Figures 2 and 3 confirms the similarities with splat caps and suggests that cooling rates following surface melting are at least as rapid as those encountered in splat quenching,[23,24] sufficient to form an extended solid solution of 6 to 7 pct silicon in aluminum.[25] Calculated cooling rates support this conjecture.[7,11] While it is not clear how mixing of the components occurs within the melted regions, material moves rapidly enough

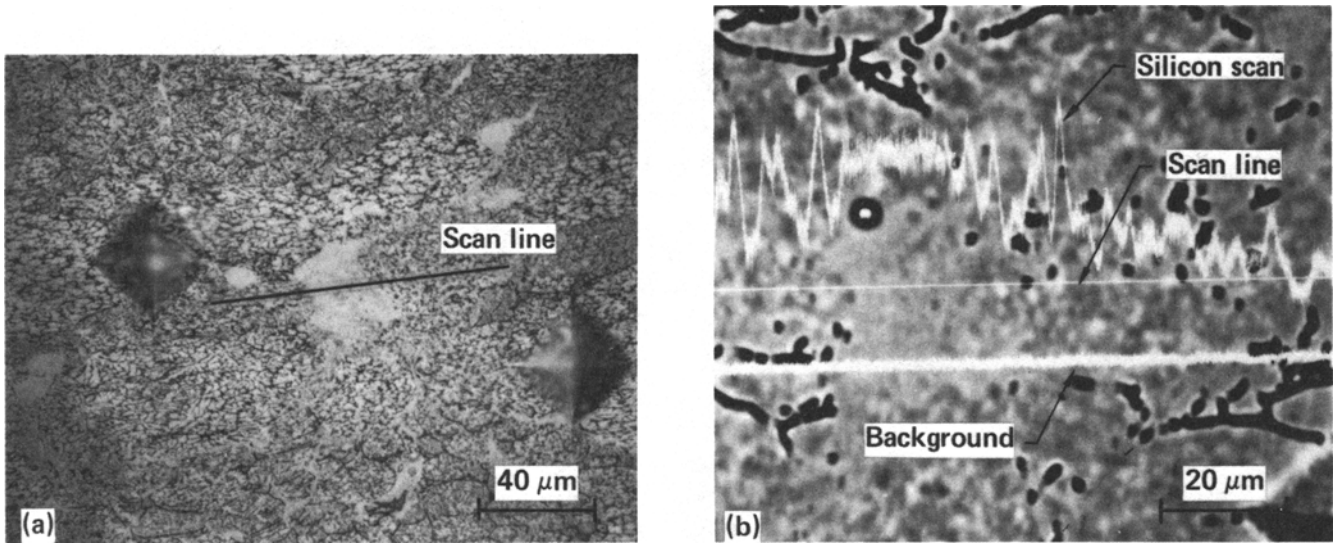


Fig. 12 — Microstructure of aluminum-6 pct silicon specimen 11P. The optical micrograph (*a*) shows a modified region and the position of the microprobe scan line. The microprobe scan in (*b*) shows that silicon is more homogeneously distributed in the modified region. This may be compared with the analysis of the splat cap given in Fig. 3.

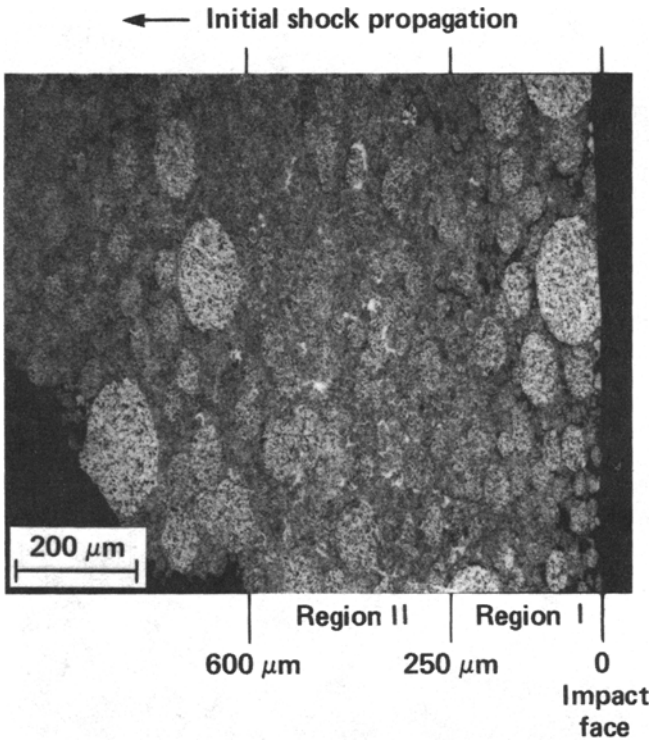


Fig. 13 — Triplex structure in aluminum-6 pct silicon specimen 11P, compacted with a mild steel cover. Locally modified material (white areas) is apparent in region II.

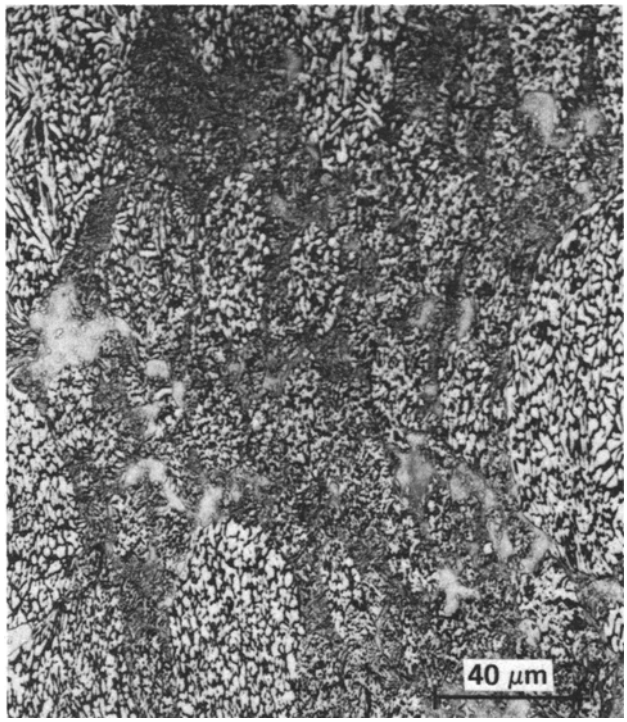


Fig. 14 — Microstructure of aluminum-6 pct silicon specimen 15P in which locally melted material forms a nearly continuous phase between powder particles that have an essentially unaltered microstructure.

initial region extends approximately 250 μm from the impact face. Thereafter, a layer containing locally melted material extends to a depth of 600 to 700 μm, as observed in the steel compacts. Local melting is not uniform through region II at this stress level (2.6 GPa) although at higher stresses (3.5 to 4.0 GPa) it produces a continuous phase between unaltered powder particles (Figure 14). The triplex structure is absent in experiments (16P, 19P) conducted without the mild steel plate.

### C. *Copper*

The results of a single experiment on the copper powder are summarized in Table VI. Although interpretation of the consolidated microstructure is hampered by the irregular shape of the powder particles and the lack of distinctive microstructural features, no ambiguous evidence for localized melting was observed. Considerable material flow is evident, however (Figure 15). The absence of local microstructural changes distinguishes the copper compacts from

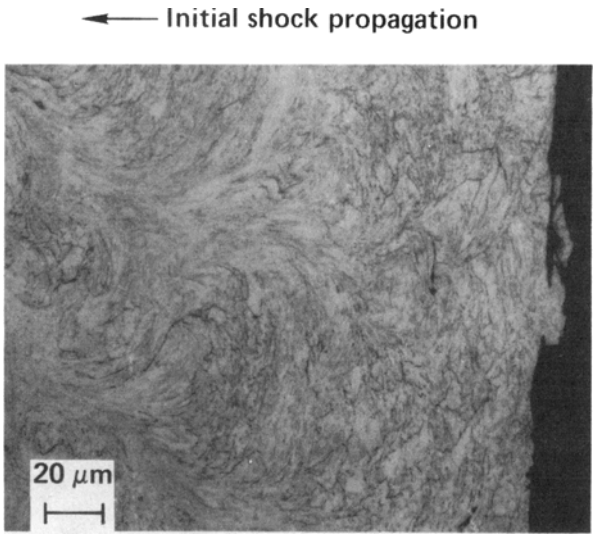


Fig. 15—Microstructure of copper specimen 10P. Considerable material flow is evident near the impact surface, which is at right.

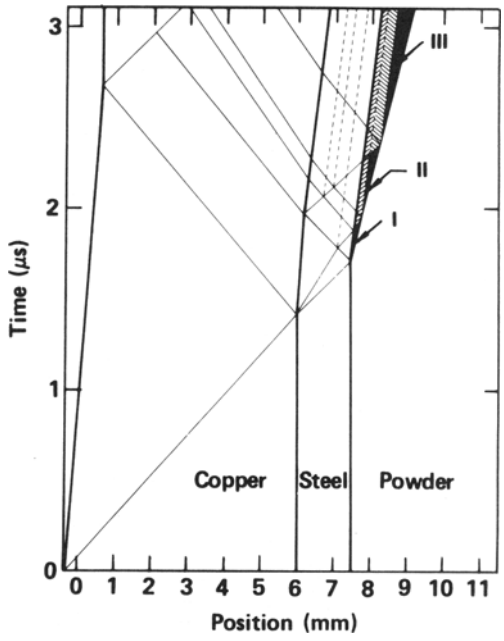


Fig. 16—Position-time diagram for 4330V specimen 2P which illustrates the formation of several regions in the compacted powder for which the deposited energy is different. These differences in energy are manifested in the microstructure as shown in Figs. 7, 8, and 13. Heavy lines denote material interfaces; light lines, shock and release wave fronts; broken lines, wave-wave interactions. The inverses of the slopes of these lines are the material and wave speeds.

those formed from either the steel or aluminum powders under similar conditions. This is primarily a result of its irregular morphology,[11] as discussed subsequently.

## IV. ANALYSIS

The distinguishing triplex structure common to specimens compacted with a mild steel cover plate is produced by a phase change in the steel cover.[11,16,19] The interactions of the various shock and release waves in the specimen as a function of time are summarized in the position-time plot shown in Figure 15. Two waves form in the steel as a result of the phase change, the faster having an amplitude of 13.0 GPa and the slower an amplitude determined by the stress in the copper driver. The 13.0 GPa wave introduces a shock in the powder sufficient to compact it to nearly solid density, but insufficient to cause significant thermal modification, thus forming region I. Because the speed of the second shock through the plate and the precompacted powder increases with shock amplitude, the thickness of region I decreases with increasing driving stresses.[19] The second wave reshocks densified material in region I, but the reshock energy, which is small relative to the energy of the initial shock,[11] is not deposited perferentially at particle boundaries and hence does not produce local effects of interest here. When the second wave catches the first, however, a single stable shock forms. The energy deposited behind this single shock is significantly greater than behind the initial wave,[11] and produces the highest surface temperatures and the greatest amount of thermal modification, region II. After the second wave has propagated some depth into the compact, release of the stress will begin. In fact, for the fixture shown in Figure 5, release will occur radially as well as axially and the details of the process do not follow the simple one-dimensional diagram of Figure 16. Nevertheless, the depth at which microstructural modification begins to decrease should be roughly constant for similar powders compacted under comparable conditions. For these experiments this is 600 to 800 $\mu$m.

The extent of microstructural modification within a region can be estimated using an energy flux model. This approach is described in detail elsewhere,[11,12,19] and only the principal features are presented here.

The energy behind the shock wave is deposited at the surface of powder particles over the rise time of the compaction shock, which is given by

$$\tau = D/v_s, \qquad [1]$$

where $D$ is a physical particle size, taken to be the median diameter,[11] and $v_s$ is the shock speed. If the powder is brought to nearly full density by the passage of the first shock wave, most of the energy is deposited by this first shock.[11] The net specific energy deposited in the powder by the compaction shock is then simply

$$E = E_s - E_r, \qquad [2]$$

where $E_s$ is energy behind the shock given by the Hugoniot relationship

$$E_s = (1/2)P(V_0 - V), \qquad [3]$$

and $E_r$ is energy upon release. Here $V_0$ is the initial specific volume, and $V$ and $P$ are the specific volume and stress behind the shock wave, determined from the powder Hugoniot.[11,20] The average flux incident on the surface of powder particles is just

$$F_0 = E/\tau A, \qquad [4]$$

where $A$ is the measured specific area of the powder. This flux is assumed to be constant and uniform for a time $\tau$, after which it falls to zero and adiabatic conditions prevail. The "typical" powder particle used in the thermal analysis is

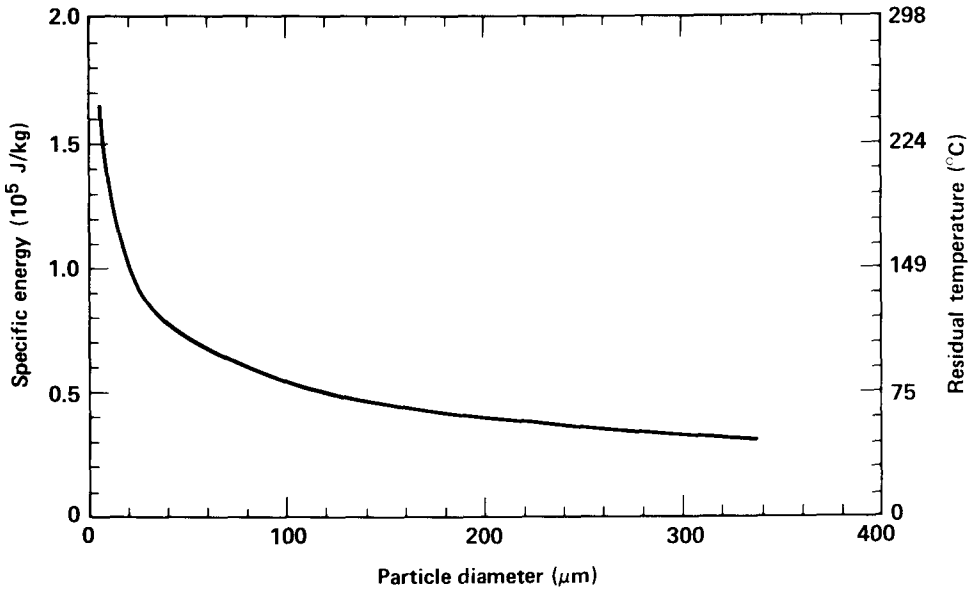


Fig. 17—Energy input required to induce surface melting as a function of the particle diameter of a hypothetical monosized 4330V powder, calculated from the energy flux model. If the residual temperature following compaction, $E/C_p$, must be less than some value to preserve the microstructure, then the minimum powder particle size is determined from this plot.

assumed to have the area equivalent diameter $\mathcal{D}$ given by

$$\mathcal{D} = 6/\rho_s A\,, \qquad [5]$$

where $\rho_s$ is the solid density. Use of $\mathcal{D}$ insures that temperatures at long times approach the average residual temperature, $E/C_p$, where $C_p$ is the specific heat. It also takes into account, through $A$, differences in powder morphology.

With these assumptions, the equation $\partial T/\partial t = \alpha \nabla T^2$, where $T$ is the temperature and $\alpha$ the thermal diffusivity, can be solved in spherical coordinates subject to the boundary condition of constant energy flux at the surface of a powder particle of diameter $\mathcal{D}$. The calculated temperatures and heating and cooling rates indicate microstructural changes that may occur. The progress of a given phase change can be determined by following its isotherm, and the volume fraction transformed can be estimated from the ratio of the volume transformed at maximum penetration of the isotherm to that of the model particle. Because it averages the energy distribution over all available powder surface area, this analysis can statistically describe the type and average extent of modification but cannot predict the detailed distribution of such changes.

This model has been applied to the experiments described here,[11] and the results are summarized in Tables IV, V, and VI. In calculating these results it was assumed that the austenite transformation for the 4330V occurs at about 807 °C[11] and that all of the austenite is retained as martensite. The eutectic temperature of 577 °C[15] was used to evaluate the aluminum-6 pct silicon specimens. Alternative use of the liquidus, 615 °C, will not significantly change the results. Considering the elementary nature of the approach, the overall agreement is good, particularly for the aluminum compacts and the steel compacts in region II, where reliable measurements of the volume fraction of transformation can be made.*

*Because the acoustical impedance of aluminum is significantly lower than that of copper or steel, the shock history in the aluminum powder is more complex than indicated in Figure 16. Hence, in Table V only an "average" region II has been included (see Reference 19).

## V. DISCUSSION

The surface temperature varies roughly as the flux $F_0$.[11] Hence, from Eq. [4] it follows that maximum local thermal modification of the microstructure occurs in spherical powders, which have small surface areas and rise times.[11] Similarly, high surface area, low density irregular powders have low surface temperatures. The results reported here are consistent with this description, and the irregular copper, while it is easily densified, shows no localized melting between powder particles at moderate stresses. Although considerable material flow and mechanical interlocking between particles occurs (Figure 15), there is no metallurgical bonding. The area-equivalent diameter for this powder is small (Table II) indicating that energy deposited at the surface is quickly diffused throughout the interior of the powder particles with little perferential heating of the surface, and surface temperatures only slightly exceed the residual temperatures (Table VI).

From a metallurgical viewpoint, one generally wishes to minimize thermally changes in the initial powder microstructure. This requires that the residual temperature, and thus the energy, be minimized subject to the constraint that the surface temperatures be high enough to yield sufficient melting for adequate interparticle bonding. For a monosized spherical powder it can be shown[11] that the maximum surface temperature increases with increasing particle diameter. This implies that the energy input required to achieve a specified degree of melting or transformation must decrease with increasing particle diameter. This is illustrated in Figure 17, which was calculated, using the energy flux model, for incipient melting at the surface of a hypothetical monosized 4330V powder particle. The corresponding residual temperatures in the consolidated body are also given. Clearly, the residual temperature must be lower than the temperature at which significant bulk modification of the powder microstructure begins. If the maximum residual temperature is fixed, the powder particle size cannot be smaller than the size determined from a plot such as Figure 17, otherwise the energy required to induce localized

melting will be too large. Although alternative bonding processes, such as diffusion bonding, may lower the energy necessary to produce a well-bonded compact, it is apparent that it may be impossible to produce desired local microstructural changes in very fine powders without altering their bulk structure. The size chosen for compaction must be a compromise between the fine size required for rapid solidification during powder manufacture on one hand and the compact properties and preservation of the power structure following consolidation on the other. A broad powder size distribution will displace the calculated curve in Figure 17 to larger energies at a given median particle size, but the form of the curve will not change.

The local microstructural changes produced in compacted specimens depend not only on the local (short time) cooling rate (controlled solely by the thermal properties of the powder material), but also on the macroscopic (long time) cooling rate (determined by the geometry and thermal properties of the surroundings as well as the compact). Rapidly solidified structures which form at particle interfaces during dynamic consolidation may be altered if the residual temperature is too high and is not dissipated quickly. The mottled appearance of some of the interparticle melt regions formed in compacts of aluminum-6 pct silicon (Figures 11, 12, and 14) and the tempered martensite character of the microstructure of sample 18P (Figure 10) may be the result of such conditions. In contrast, the residual temperatures in the steel compacts (Table IV) can exceed the martensite formation temperature, $M_s$ (Table I), even in those regions where localized martensite has clearly formed (Figures 7 and 8). A simple calculation[27] shows that a compact 3 mm thick will come into thermal equilibrium with its surroundings in times of the order of 0.3 to 1 seconds. This is rapid enough to form martensite in the 4330V provided that the equilibrium temperature is below the $M_s$ temperature.[28] The conditions which prevail long after compaction has occurred are not known in detail, however, and a realistic assessment of the macroscopic cooling rates is difficult to make. It is not clear why specimens compacted under similar circumstances have microstructures which indicate significantly different macroscopic cooling rates (compare Figures 8 and 10).

## VI. SUMMARY AND CONCLUSIONS

Powders of 4330V steel, aluminum-6 pct silicon alloy, and copper have been dynamically consolidated under well-characterized conditions. The microstructures of the compacts have been described and analyzed in terms of an energy flux model for energy deposition at powder particle interfaces. It is concluded that:

1. Knowledge of the shock history is essential to the interpretation and control of the microstructure of the consolidated body.
2. For the steel and aluminum-6 pct silicon powders, both of which have a basically spherical morphology, the compaction shock energy is primarily deposited at the surfaces of powder particles during consolidation, and dissipates *via* thermal diffusion. Martensite formation and melting, respectively, occur locally near particle interfaces.
3. No local microstructural modifications are observed in compacts formed from irregular copper powder. This result is consistent with predictions based on the energy flux description of energy deposition during consolidation.
4. Cooling rates at powder particle surfaces can be as high as those achieved during splat quenching, consistent with the formation of a homogeneous distribution of silicon observed in locally melted regions of aluminum-6 pct silicon alloy compacts. The macroscopic cooling rate may also determine in part the microstructure of the final compact.
5. Residual temperatures following compaction at stresses sufficiently high to induce desired surface modifications may produce undesirable changes in the final compact microstructure. The minimum powder particle size suitable for dynamic compaction is fixed by the maximum residual temperature.

## ACKNOWLEDGMENTS

The author extends his sincere thanks to S. L. Weinland, F. Helm, and T. Sullivan who assembled and helped to perform many of the experiments. J. E. Smugeresky provided much helpful advice as well as (for the price of two beers) Figure 3. Microprobe analyses were performed by D. McCoy and J. Balser. This work was supported in part by the United States Army Research Office and performed under the auspices of the United States Department of Energy by the Lawrence Livermore National Laboratory under contract No. W-7405-ENG-48.

## REFERENCES

1. D. Raybould, D. G. Morris, and G. A. Cooper: *J. Mat. Sci.*, 1979, vol. 14, pp. 2523-26.
2. D. Raybould: in *Shock Waves and High-Strain-Rate Phenomena in Metals*, M. A. Meyers and L. E. Murr, eds., Plenum Press, New York, NY, 1981, pp. 895-911.
3. D. Raybould: *J. Mat. Sci.*, 1981, vol. 16, pp. 589-98.
4. D. Raybould: *Powder Metallurgy*, 1980, vol. 23, pp. 37-44.
5. D. G. Morris: *Metal Science*, 1982, vol. 16, pp. 457-64.
6. W. H. Gourdin and J. E. Smugeresky: *Proceedings of the Third Conference on Rapid Solidification Processing: Principles and Technologies*, Gaithersburg, MD, December 6-8, 1982, R. Mehrabian, ed., National Bureau of Standards, 1983, pp. 565-71.
7. D. G. Morris: *Metal Science*, 1981, vol. 15, pp. 116-24.
8. D. G. Morris: *Metal Science*, 1980, vol. 14, pp. 215-20.
9. D. G. Morris: *J. Mat. Sci.*, 1982, vol. 17, pp. 1789-94.
10. M. A. Meyers, B. B. Gupta, and L. E. Murr: *Journal of Metals*, October 1981, pp. 21-26.
11. W. H. Gourdin: *Journal of Applied Physics*, 1984, vol. 55, pp. 172-81.
12. W. H. Gourdin: *Shock Waves in Condensed Matter—1983* (Proceedings of the American Physical Society 1983 Topical Conference on Shock Waves in Condensed Matter, Sante Fe, NM, July 18-21, 1983), J. R. Asay, R. A. Graham, and G. K. Straub, eds., Elsevier, 1984, pp. 379-82.
13. W. H. Gourdin: *Materials Science and Engineering*, in press.
14. W. F. Smith: *Structures and Properties of Engineering Alloys*, McGraw-Hill, New York, NY, 1981, p. 148.
15. W. F. Smith: *ibid.*, pp. 201-06.
16. L. M. Barker and R. E. Hollenbach: *J. Appl. Phys.*, 1974, vol. 45, pp. 4872-87.
17. B. M. Dobratz: *LLNL Explosives Handbook*, University of California, Lawrence Livermore National Laboratory, UCRL-52997, March 16, 1981.

18. E. L. Lee: Lawrence Livermore National Laboratory, Department of Chemistry and Materials Science, P.O. Box 808, L-368, Livermore, CA 94550, private communication, 1982.
19. W. H. Gourdin: University of California, Lawrence Livermore National Laboratory, UCRL-88902, May 1983.
20. W. H. Gourdin and S. L. Weinland: *Shock Waves in Condensed Matter—1983* (Proceedings of the American Physical Society 1983 Topical Conference on Shock Waves in Condensed Matter, Sante Fe, NM, July 18-21, 1983), J. R. Asay, R. A. Graham, and G. K. Straub, eds., Elsevier, 1984, pp. 99-102.
21. D. G. Morris: *Materials Science and Engineering*, 1983, vol. 57, pp. 187-95.
22. W. F. Smith: *ibid.*, p. 36.
23. P. Predecki, A. W. Mullendore, and N. J. Grant: *Trans. TMS-AIME*, 1965, vol. 233, pp. 1581-86.
24. R. C. Ruhl: *Mat. Sci. and Eng.*, 1967, vol. 1, pp. 313-20.
25. M. Itagaki, B. C. Giessen, and N. J. Grant: *Trans. ASM*, 1968, vol. 61, pp. 330-35.
26. D. Raybould: *Inter. J. Pow. Met. and Pow. Tech.*, 1980, vol. 16, pp. 9-19.
27. H. S. Carslaw and J. C. Jaeger: *Conduction of Heat in Solids*, 2nd ed., Oxford University Press, Oxford, 1959, pp. 53-56.
28. *Aerospace Structural Metals Handbook*, Mechanical Properties Data Center, Battelle Columbus Laboratories, 1982.